nature geoscience

LETTERS

PUBLISHED ONLINE: 26 SEPTEMBER 2010 | DOI: 10.1038/NGEO959

Holocene changes in the position and intensity of the southern westerly wind belt

Frank Lamy[1]*, Rolf Kilian[2], Helge W. Arz[3], Jean-Pierre Francois[4], Jérôme Kaiser[5], Matthias Prange[6] and Tatjana Steinke[1,2]

The position and intensity of the southern westerly wind belt varies seasonally as a consequence of changes in sea surface temperature. During the austral winter, the belt expands northward and the wind intensity in the core decreases. Conversely, during the summer, the belt contracts, and the intensity within the core is strengthened. Reconstructions of the westerly winds since the last glacial maximum, however, have suggested that changes at a single site reflected shifts throughout the entire southern wind belt[1–4]. Here we use sedimentological and pollen records to reconstruct precipitation patterns over the past 12,500 yr from sites along the windward side of the Andes. Precipitation at the sites, located in the present core and northern margin of the westerlies, is driven almost entirely by the wind belt[5], and can be used to reconstruct its intensity. Rather than varying coherently throughout the Holocene epoch, we find a distinct anti-phasing of wind strength between the core and northern margin over multi-millennial timescales. During the early Holocene, the core westerlies were strong whereas the northern margin westerlies were weak. We observe the opposite pattern in the late Holocene. As this variation resembles modern seasonal variability, we suggest that our observed changes in westerly wind strength can best be explained by variations in sea surface temperature in the eastern South Pacific Ocean.

Chile is ideally located to reconstruct past variability of the southern westerly wind belt (SWW) as the SWW almost entirely controls precipitation on the western side of the Andes in southern South America with an extreme north–south rainfall gradient from the semiarid, winter-rain climate in central Chile to year-round hyper-humid conditions in the fjord region of southern Chile[5] (Supplementary Fig. S1). Therefore, any paleoclimatic proxy record primarily controlled by rainfall changes is suitable for reconstructing past changes in the SWW in this region. In present-day austral winters, the SWW extends northward, providing rainfall to central Chile (33°–40° S), but zonal winds are reduced in its core zone in southernmost Chile (50°–55° S; Fig. 1a). During austral summer, the zonal wind pattern shows a latitudinally more confined and intensified SWW with maxima over southernmost Chile (Fig. 1b). Previous reconstructions of the SWW were primarily based on single sites and generally suggested a northward migration and intensification of the SWW during colder periods[1,2,4]. Intensity variations across the wind belt have only recently been addressed and interpreted in terms of co-varying moisture changes in southern and central Chile over the Holocene[3]. However, this inference is only based on two single pollen records, located at 41° S and 51° S, from which the southern record (Paine; Fig. 1d) misses a straightforward relation to westerly wind strength changes similar to other records on the eastern side of the Andes (for example, Potrok Aike[2]; Fig. 1d; Supplementary Discussion S1).

The present SWW core is centred at ~50°–55° S, where annual precipitation reaches very high values on the windward side (3,000–10,000 mm), with a summer maximum correlating to stronger westerly winds (Fig. 1a,b; ref. 6). Our multi-millennial-scale Holocene SWW reconstruction is based on three marine sediment cores, one lacustrine record, and a peat-bog pollen record from different sites along the fjord system near the westernmost Strait of Magellan (~53° S) and from the Skyring fjord east of the Andean climate divide (Fig. 1d). The records have well constrained age-models (Supplementary Table S1) based on radiocarbon dating and the occurrence of regional ash layers during the Holocene[7]. Depending on the individual setting, our rainfall and wind strength reconstructions are based on different proxies (Supplementary Discussion S2).

From the Skyring fjord system east of the Andean crest, we provide a record of wind-induced long-distance transport (>100 km) of illite and chlorite-rich clays with a clear Andean signature (Fig. 2b; Supplementary Fig. S2). We interpret this record directly in terms of westerly wind strength largely independent of precipitation changes. At site Palm2, we use strong fluctuations of biogenic carbonate accumulation-rates (AR) as a proxy for salinity changes in superficial fjord waters (Fig. 2c). Today, lower salinities occur during times of elevated precipitation and stronger winds that keep the low-salinity fjord waters inside and diminish the open marine influence on the fjord system, reducing biogenic carbonate production. At fjord Site TM1, we use AR of siliciclastic components (Fig. 2d) and terrestrial organic carbon (Fig. 2e) as recorders for fluvial supply. These records are complemented by terrestrial organic carbon AR data (Fig. 2f) from core TML1 retrieved from nearby located Lake Tamar. Core TML1 contains several terrestrial mass flow layers deposited during extreme early Holocene rainfall events (Fig. 2f; Supplementary Fig. S3). Our pollen data from Lake Tamar support the idea of an underlying climatic driving mechanism in the genesis of the mass flow layers, and offer additional precipitation and wind strength-related proxy records (Fig. 2g; Supplementary Figs S4 and S5). From close to the rainfall maximum at the Gran Campo Nevado mountain range, we further include a peat-bog pollen record (GC2) of the

[1]Alfred Wegener Institut für Polar- und Meeresforschung, Am Alten Hafen 26, 27568 Bremerhaven, Germany, [2]Lehrstuhl für Geologie, Fachbereich Geowissenschaften (FB VI), Universität Trier, 54286 Trier, Germany, [3]Leibniz Institute for Baltic Sea Research Warnemünde, Seestraße 15, 18119 Rostock-Warnemünde, Germany, [4]Seminar für Geographie und ihre Didaktik, Universität Köln, Gronewaldstr 2, 50931 Köln, Germany, [5]UMR 7159 LOCEAN, Université Pierre et Marie Curie, 4 place Jussieu, 75252 Paris, France, [6]MARUM Center for Marine Environmental Sciences and Department of Geosciences, University of Bremen, 28334 Bremen, Germany. *e-mail: Frank.Lamy@awi.de.

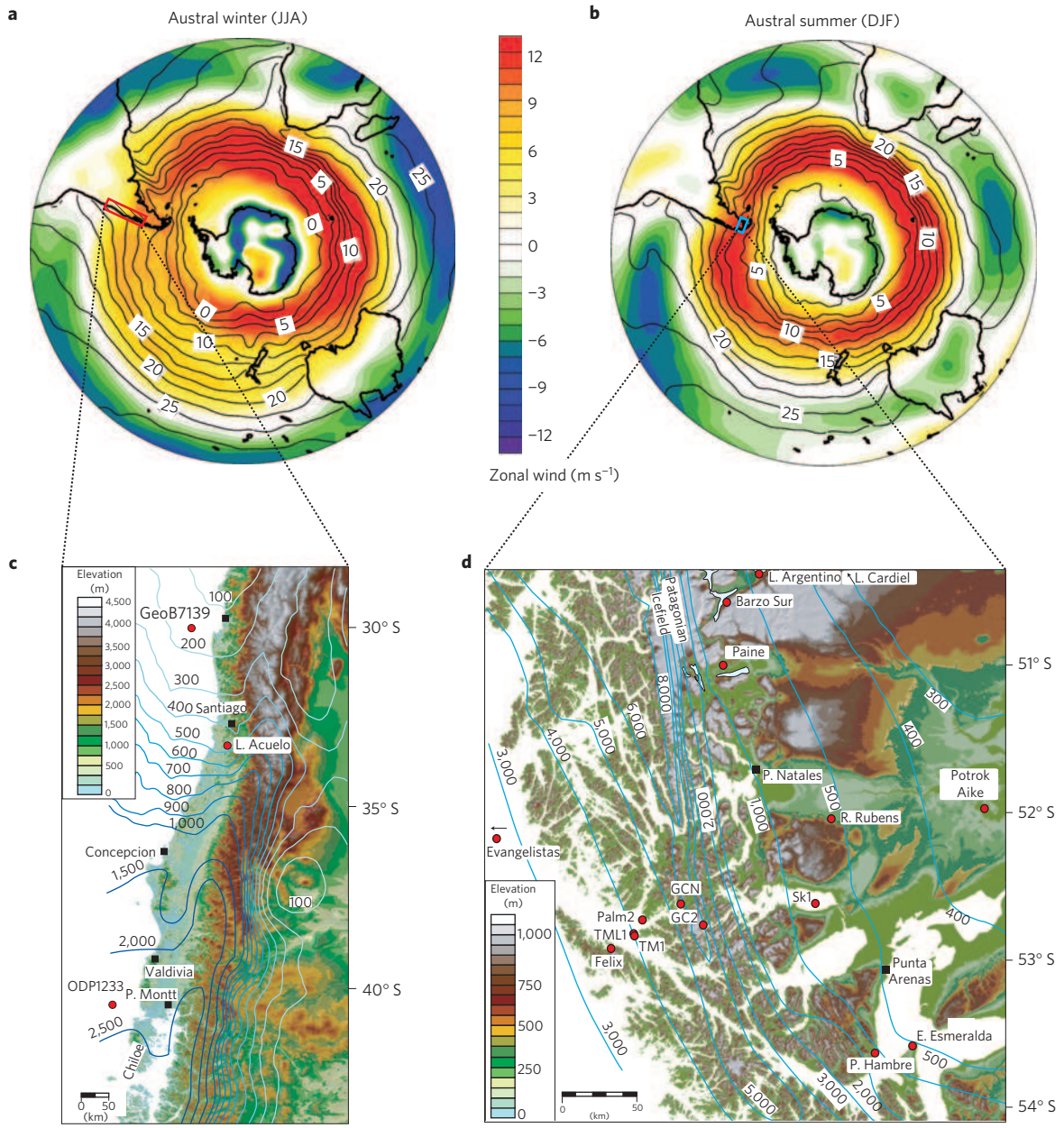

Figure 1 | Modern climatology and setting. a, SH zonal wind (m s^{-1}) climatology at 850 hPa for austral winter and **b**, austral summer based on NCEP/NCAR reanalysis data[27]. Overlaid isotherms are climatological sea surface temperatures (°C) for the corresponding seasons based on the NODC World Ocean Atlas (1998). **c**, Topographic map of central Chile with annual precipitation in millimetres (ref. 28) (primarily winter-rain) and the location of paleoclimate records discussed in the text. **d**, Topographic map of southernmost Chile with annual precipitation in millimetres (refs 6,28) and the location of paleoclimate records discussed in the text.

percentage of hygrophytic taxa (Fig. 2f) as a sensitive proxy for Holocene precipitation changes in extremely humid environments (Supplementary Figs S6 and S7).

Despite individual differences between the records due to potential local overprints and the very diverse nature of the different proxies (Supplementary Discussion S2), our SWW core zone records show a clear multi-millennial pattern (Fig. 2). Most records reveal a trend towards wetter/windier conditions starting at ~12.5 thousand year before present (kyr BP), a maximum between ~12 and ~8.5 kyr BP, intermediate conditions thereafter until ~5.5 kyr BP, and finally reduced precipitation and less intense westerlies during the late Holocene. Previous reconstructions within the SWW core zone were primarily based on pollen records from southeast Patagonia (for example, Potrok Aike[2], Paine[3]; Fig. 1d) and are partly inconsistent with our results. However, all previous reconstructions in this latitudinal band were based on records from the lee side of the Andes where other than westerly related rainfall sources become more important[8]. Moreover, plant communities at the dry lee side respond rather indirectly to SWW changes, as wind-induced dry stress is a major ecological factor in this region[9]. Such an interpretation may reconcile inconsistencies with our records (Supplementary Discussion S1).

At the northern margin of the SWW in central Chile (Fig. 1c), reconstructed rainfall changes are generally antiphased to those in the core zone in southern Chile. Figure 2a shows a rainfall reconstruction based on the hydrological balance of Lake Aculeo, located in the winter-rain domain at ~34° S (ref. 10). Although the record only reaches back to ~10 kyr BP, substantially lower rainfall

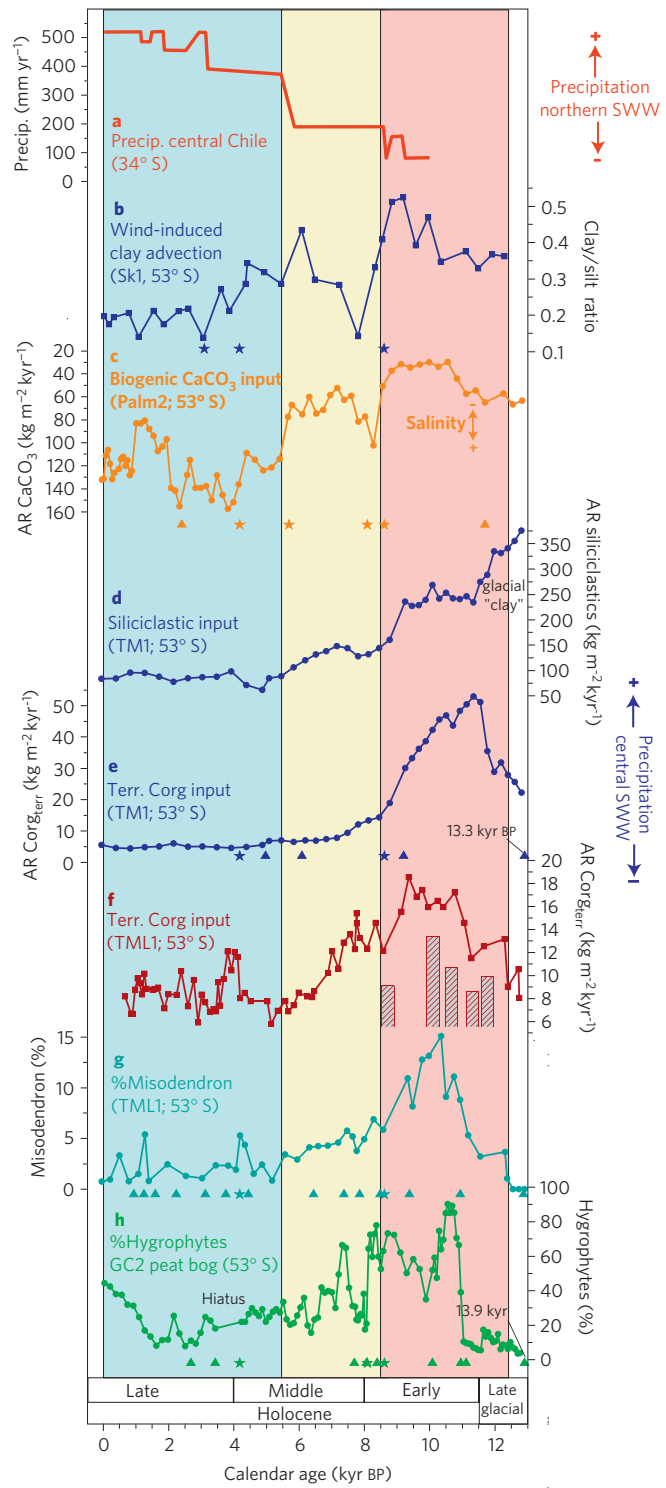

Figure 2 | Proxy records for precipitation and wind strength in the core SWW (~53° S) and at the northern SWW margin (~34° S). a, Rainfall reconstruction from Lake Aculeo[10]. **b**, Clay/silt ratios from core Sk1. **c**, Biogenic carbonate AR from core Palm2 (reversed *y*-scale). **d**, AR of siliciclastic material at site TM1 and **e**, terrestrial organic carbon ($Corg_{terr}$)AR from core TM1. **f**, $Corg_{terr}$ AR from core TML1. Vertical bars indicate the occurrence and thickness (13–34 cm) of terrestrial mass flow layers. **g**, Relative pollen percentages of Misodendron (core TML1). **h**, Pollen percentage of hygrophytic taxa (core GC2). Triangles indicate radiocarbon dates and stars ash-layers. Coloured bars distinguish the early (red), middle (yellow), and late Holocene (blue) multi-millennial phases in the evolution of the SWW.

during the early Holocene, and thus reduced westerly influence, has been reconstructed in the whole central Chilean region south to the Chilean Lake district and Chiloe[11] (Supplementary Discussion S1). Especially after ~5.5 kyr BP, rainfall substantially increases at Lake Aculeo (Fig. 2a) and also most other central Chilean records reveal wetter conditions coinciding with drier and less windy conditions in the southern fjords (Fig. 2).

This emerging pattern of antiphased intensity changes of the SWW in the centre and northern margin strongly resembles the observed changes over the present seasonal cycle (Fig. 1a,b). This analogy suggests that the early Holocene was characterized by mean more summer-like conditions of the westerlies versus a more winter-like pattern in the late Holocene. Surface westerlies result from the meridional transport of westerly momentum by transient eddies which acts against losses by surface friction[12]. The eddies, in turn, are driven by the potential energy available in the meridional temperature gradients[13]. In the ocean-dominated southern hemisphere (SH), eddy activity, momentum flux convergence and hence the strength and position of the SWW are therefore primarily controlled by sea surface temperatures (SST) (Fig. 1a,b).

The early Holocene SWW core maximum coincides with a widespread warming at SH mid-latitudes, as evidenced by SST records from the Atlantic sector (53° S; ref. 14; Fig. 3f) as well as offshore central (ODP Site 1233; 41° S) and northern Chile (Site GeoB7139; 30° S; refs 4,15; Fig. 3d,e). The pronounced mid-latitude ocean surface warming supports a summer-like early Holocene scenario, as modern SST observations reveal the strongest summer warming between 20° S and 50° S (Supplementary Fig. S8). At the same time, SSTs in the eastern tropical Pacific were relatively cold[16] (Fig. 3c), reducing the mid- to low latitude SST gradient in the South Pacific. This pattern would be consistent with reduced early Holocene westerlies at their northern margin, as it appears at present during summer when the SST gradient between mid latitudes and the equator is at a minimum (Supplementary Fig. S8).

The SH early Holocene thermal maximum and coinciding SWW enhancement in the centre of the wind belt is difficult to explain by orbital forcing, as SH summer insolation was at a minimum (Fig. 3h). Although some climate models produce warmer-than-present annual-mean SSTs in the early Holocene South Pacific in response to orbital forcing[17], the simulated temperature anomalies are much smaller than those suggested by the proxy records. Additional SH warming during the early Holocene might be attributable to changes in the global ocean circulation which involve a bipolar seesaw-like surface temperature pattern. A response of the SWW to changes in the Atlantic meridional overturning circulation (AMOC) strength has been previously proposed for Termination 1 (ref. 4). For the early Holocene, such a mechanism has been invoked for explaining warm temperatures in the Southern Ocean and Antarctica[18] and is consistent with a reconstruction of the AMOC strength in the North Atlantic[19] (Fig. 3b). This explanation implies that the AMOC reduction, starting with melt-water input during the northern hemisphere Younger Dryas, combines with the early Holocene final melting of the Laurentian ice-sheet to induce the temperature maximum extending from ~12.5 to ~8.5 kyr BP in the south. The warming may have been amplified by reduced sea-ice cover in the Southern Ocean, consistent with paleodata[14].

The late Holocene cooling in the SH mid-latitudes (Fig. 3d,e) and more modern winter-like SWW pattern coincide with progressive warming of the eastern tropical Pacific (Fig. 3c) enhancing the mid- to low latitude SST gradient in the ocean basin (Fig. 3g,h). The tropical Pacific warming can be interpreted in terms of a southward movement of the Pacific Intertropical Convergence Zone enhancing atmospheric pressure gradients at the northern margin of the SWW, consistent with the suggested strengthening there. The late Holocene time-interval probably corresponds to mean more El Niño-like conditions[20]. The impact

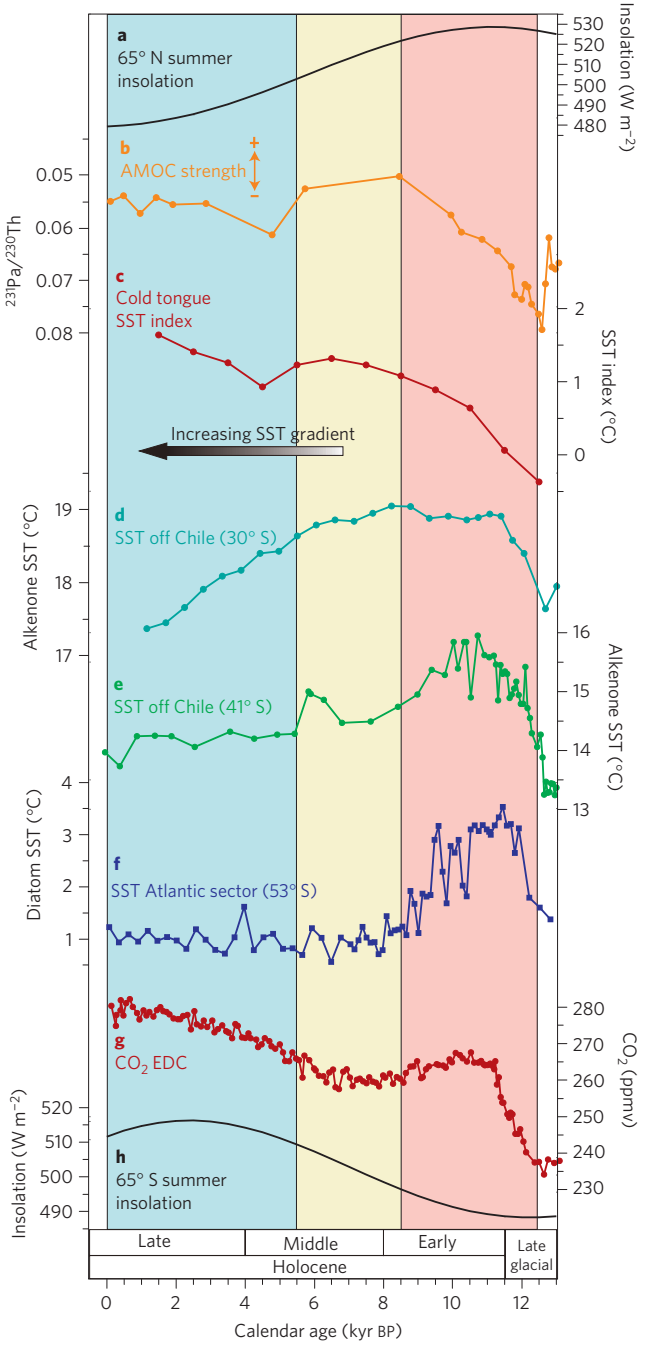

Figure 3 | Compilation of paleoclimatic records to explain Holocene SWW changes. a, Summer insolation (21 June) at 65° N (ref. 29). **b**, $^{231}Pa/^{230}Th$ record from a subtropical North Atlantic sediment core taken as a proxy for the strength of the Atlantic meridional overturning circulation[19]. **c**, Composite alkenone SST index from the eastern Pacific equatorial cold tongue[16]. **d**, Alkenone SST record from the Chilean margin at ~30° S (ref. 15). **e**, Alkenone SST record from the Chilean margin at ~41° S (ref. 4). **f**, Diatom assemblage-based summer SST record from the Atlantic sector of the Southern Ocean at ~53° S (ref. 14). **g**, CO_2 record from the EDC ice-core[24]. **h**, Summer insolation (21 December) at 65° S (ref. 29). Coloured bars as in Fig. 2.

of mean more El Niño-like conditions on the SWW is consistent with our data, as the late Holocene enhancement of rainfall at the northern margin of the SWW and concurrent reduction in the centre exactly fits the modern precipitation pattern during El Niño events[21].

Our comparison of SWW records from the northern margin and the central part of the wind belt suggests antiphased intensity changes in both regions. This pattern has implications for reconstructions of the glacial westerlies, which are mainly based on proxy records from the northern margin of the SWW (refs 1,4). Although we cannot reconstruct meridional shifts of the central SWW, as our records only cover a small latitudinal band in the south, the analogy to modern seasonal changes implies that a latitudinal expansion of the SWW during cold phases ('winter-like') and contraction during warm climate conditions ('summer-like') may have been likewise important for the behaviour of the SWW on glacial/interglacial time-scales and over glacial millennial-scale fluctuations. Meridional shifts and intensity changes of the SWW have been related to changes in Southern Ocean ventilation affecting atmospheric carbon dioxide (CO_2) content[22]. Although such an impact of the SWW has been recently doubted, based on modelling studies[23], the similar timing of the SWW and CO_2 proposed for Termination 1 (refs 4,22) appears to extend into the early Holocene. The intensification and latitudinal compression of the SWW based on our reconstruction parallels the early Holocene CO_2 maximum shown in ice-cores[24] (Fig. 3g), consistent with enhanced ocean ventilation. This connection breaks down in the middle and late Holocene, during which the CO_2 content was probably no longer controlled primarily by Southern Ocean processes[25].

Independent of any potential SWW-atmospheric CO_2 relation, the early Holocene strengthening of the SWW in the centre and its reduction at the northern margin may serve as an analogue for future climate patterns under warmer-than-present conditions. If this analogy is valid, our results suggest substantial rainfall reductions in the highly populated winter-rain zone of Chile over the coming centuries, consistent with model results for future climate scenarios[26].

Methods

The fjord and lake sediment cores were retrieved with a UWITEC piston corer from platforms during various cruises aboard the R/V Gran Campo II. To ensure the recovery of modern sediment surfaces, short gravity cores from the same core location have been appended to the top of piston cores (up to 18 cm, correlation through physical properties data). The peat bog core GC2 was obtained with a Russian and a Wardenaar corer. The methods used vary among the individual records. We have therefore included information on the methods applied in the supplementary discussion of the records (Supplementary Discussion S2).

Received 22 November 2009; accepted 12 August 2010; published online 26 September 2010

References

1. Heusser, C. J. Southern Westerlies during the Last Glacial Maximum. *Quat. Res.* **31,** 423–425 (1989).
2. Mayr, C. *et al.* Holocene variability of the Southern Hemisphere westerlies in Argentinean Patagonia (52° S). *Quat. Sci. Rev.* **26,** 579–584 (2007).
3. Moreno, P. I., Francois, J. P., Moy, C. M. & Villa-Martinez, R. Covariability of the Southern Westerlies and atmospheric CO_2 during the Holocene. *Geology* **38,** 727–730 (2010).
4. Lamy, F. *et al.* Modulation of the bipolar seesaw in the Southeast Pacific during Termination 1. *Earth Planet. Sci. Lett.* **259,** 400–413 (2007).
5. Garreaud, R. D. Precipitation and circulation covariability in the extratropics. *J. Clim.* **20,** 4789–4797 (2007).
6. Schneider, C. *et al.* Weather observations across the Southern Andes at 53° S. *Phys. Geogr.* **24,** 97–119 (2003).
7. Kilian, R., Hohner, M., Biester, H., Wallrabe-Adams, H. J. & Stern, C. R. Holocene peat and lake sediment tephra record from the southernmost Chilean Andes (53–55° S). *Rev. Geol. Chile* **30,** 23–37 (2003).
8. Wagner, S. *et al.* Transient simulations, empirical reconstructions and forcing mechanisms for the Mid-holocene hydrological climate in southern Patagonia. *Clim. Dyn.* **29,** 333–355 (2007).
9. Endlicher, W. Patagonien–Klima- und agrarökologische Probleme an der Magellanstraße. *Geogr. Rundschau* **43,** 143–151 (1991).
10. Jenny, B., Wilhelm, D. & Valero-Garces, B. L. The Southern Westerlies in Central Chile: Holocene precipitation estimates based on a water balance model for Laguna Aculeo (33° 50′ S). *Clim. Dyn.* **20,** 269–280 (2003).
11. Latorre, C. *et al.* in *The Geology of Chile* (eds Moreno, T. & Gibbons, W.) 309–328 (The Geological Society, 2007).

12. Trenberth, K. E. The role of eddies in maintaining the Westerlies in the Southern Hemisphere winter. *J. Atmos. Sci.* **44,** 1498–1508 (1987).
13. Gill, A. E. *Atmosphere-Ocean Dynamics* (Academic, 1982).
14. Bianchi, C. & Gersonde, R. Climate evolution at the last deglaciation: The role of the Southern Ocean. *Earth Planet. Sci. Lett.* **228,** 407–424 (2004).
15. Kaiser, J., Schefuss, E., Lamy, F., Mohtadi, M. & Hebbeln, D. Glacial to Holocene changes in sea surface temperature and coastal vegetation in north central Chile: High versus low latitude forcing. *Quat. Sci. Rev.* **27,** 2064–2075 (2008).
16. Koutavas, A. & Sachs, J. P. Northern timing of deglaciation in the eastern equatorial Pacific from alkenone paleothermometry. *Paleoceanography* **23,** PA4205 (2008).
17. Liu, Z., Brady, E. & Lynch-Stieglitz, J. Global ocean response to orbital forcing in the Holocene. *Paleoceanography* **18,** 1041 (2003).
18. Masson, V. *et al.* Holocene climate variability in Antarctica based on 11 ice-core isotopic records. *Quat. Res.* **54,** 348–358 (2000).
19. McManus, J., Francois, R., Gherardi, J-M., Kelgwin, L. D. & Brown-Leger, S. Collapse and rapid resumption of Atlantic meridional circulation linked to deglacial climate changes. *Nature* **428,** 834–837 (2004).
20. Cane, M. A. The evolution of El Nino, past and future. *Earth Planet. Sci. Lett.* **230,** 227–240 (2005).
21. Schneider, C. & Gies, D. Effects of El Nino-southern oscillation on southernmost South America precipitation at 53° S revealed from NCEP-NCAR reanalyses and weather station data. *Int. J. Clim.* **24,** 1057–1076 (2004).
22. Anderson, R. F. *et al.* Wind-driven upwelling in the Southern Ocean and the deglacial rise in atmospheric CO_2. *Science* **323,** 1443–1448 (2009).
23. Tschumi, T., Joos, F. & Parekh, P. How important are Southern Hemisphere wind changes for low glacial carbon dioxide? A model study. *Paleoceanography* **23,** PA4208 (2008).
24. Monnin, E. *et al.* Evidence for substantial accumulation rate variability in Antarctica during the Holocene, through synchronization of CO_2 in the Taylor Dome, Dome C and DML ice cores. *Earth Planet. Sci. Lett.* **224,** 45–54 (2004).
25. Brovkin, V., Kim, J. H., Hofmann, M. & Schneider, R. A lowering effect of reconstructed Holocene changes in sea surface temperatures on the atmospheric CO_2 concentration. *Glob. Biogeochem. Cycles* **22,** GB1016 (2008).
26. Vera, C., Silvestri, G., Liebmann, B. & Gonzalez, P. Climate change scenarios for seasonal precipitation in South America from IPCC-AR4 models. *Geophys. Res. Lett.* **33,** L13707 (2006).
27. Kalnay, E. *et al.* The NCEP/NCAR 40-year reanalysis project. *Bull. Am. Meteorol. Soc.* **77,** 437–471 (1996).
28. New, M., Lister, D., Hulme, M. & Makin, I. A high-resolution data set of surface climate over global land areas. *Clim. Res.* **21,** 1–25 (2002).
29. Berger, A. & Loutre, M. F. Insolation values for the climate of the last 10 million years. *Quat. Sci. Rev.* **10,** 297–317 (1991).

Acknowledgements

We thank R. Gersonde and R. Tiedemann for comments and suggestions. M. Arevalo and O. B. Urrea are acknowledged for technical and logistic support during various campaigns with RV Gran Campo II and laboratory work in Trier, respectively. Financial support was made available through the GFZ-Potsdam, the Gary Comer Science and Education Foundation (CSEF) as well as through DFG grants AR 367/6-1, Ki-456/10, and La 1273/7-1.

Author contributions

All authors interpreted the results and contributed to the final manuscript. F.L. and R.K. wrote the final version of the manuscript. J-P.F. performed the pollen analyses. H.W.A. and T.S. carried out most of the remaining analytical work. M.P. contributed climatological background data and analyses.

Additional information

The authors declare no competing financial interests. Supplementary information accompanies this paper on www.nature.com/naturegeoscience. Reprints and permissions information is available online at http://npg.nature.com/reprintsandpermissions. Correspondence and requests for materials should be addressed to F.L.

nature geoscience

SUPPLEMENTARY INFORMATION

DOI: 10.1038/NGEO959

Supplementary Information Lamy et al.
"Holocene changes in the position and intensity of the Southern Westerly wind belt"

Supplementary Information

Supplementary Discussion 1 and 2, Supplementary Figs S1-S8, Supplementary Table S1

Supplementary Discussion 1

Discussion on previously published Holocene westerly wind strength records from southern Patagonia

Southern Patagonia is the only continental area located within the present core of the southern westerly wind belt (SWW) (Fig. 1). Therefore, there have been numerous recent attempts to reconstruct Holocene changes of the SWW based on terrestrial records in this region (see Fig. 1d for site locations). These include for example data-sets from Laguna Potrok Aike[1,2] and Lago Cardiel[3-5] located within the semi-arid part of Argentinean Patagonia. Furthermore, records are available from Lago Argentino (Brazo Sur[6]) close to the eastern margin of the Southern Patagonian Ice Field and from the Torres del Paine National Park area (TDP) close to the Andean crest (and thus the climate divide) but already on the lee-side of the mountain range[7-9].

In this region the transition from Andean forest to Patagonian steppe is approximately located at the 500 mm annual precipitation isohyet. At similar latitudes in the Northern Hemisphere such precipitation amounts generally lead to the formation of dense forest vegetation. In contrast, in the Patagonian steppe plant-available moisture is strongly controlled by evaporation which is influenced by temperature and in particular wind speed (see figure below). The relatively short-term meteorological data at TDP are partly consistent with the ~100 yr-long meteorological time-series at Punta Arenas[10-12]. Punta Arenas and other weather stations to the east of the Andes (Puerto Natales, Torres del Paine and Lago Argentino) show a pronounced maximum in wind speed during summer, whereas no clear seasonal pattern is apparent for precipitation and thus no clear westerly wind-precipitation relationship. While the Punta Arenas station at 53°S shows a subtle precipitation maximum in summer, the stations at Puerto Natales and Paine Park (51°30'S to 51°S) show a slight maximum in autumn (March to May). In contrast, the Lago Argentino station located only slightly further to the north at 50°30'S displays a clear winter maximum in precipitation[13]. In any case, vegetation in this forest-steppe transition zone (and even more further to the east) suffers often drought stress, especially during the growing season (spring and summer)[14]. Due to this strong evaporation impact, soils become extremely dry during the growing season and lagoons fall dry in summer which can be for example observed in the extended moraine belt around the eastern Strait of Magellanes, whereas they are partly water-filled in winter. River run-offs which are not influenced by glacier or snow melt are also lowest in summer.

Paleohydrological reconstructions have been performed on records from Laguna Potrok Aike[2] assuming an anti-correlation of local hydrology to westerly wind strength. However, climate modelling and modern climatological considerations by Wagner et al.[15] show that the local pattern at Laguna Potrok Aike are rather complicated through the varying influences of precipitation changes (primarily of Atlantic origin) and evaporation variability (primarily induced by changes in westerly wind strength). Furthermore, Mayr et al.[1] use the amount of far-distance transported pollen presumably originating from the Andes further to the west (Andean Forest Taxa; AFZ) as a westerly wind strength proxy. They claim an enhancement of AFT at ~9.2 kyr BP. Based on their Fig. 2a, we would suggest that the increase in AFT occurs abruptly at ~8.7 kyr BP and lasts until ~7.2 kyr BP. The younger part of the records does not reveal any long-term trend and is dominated by strong short-term variability which is not the focus of our paper. Mayr et al also show a comparison to the AFT at the Rio Rubens Bog site[16]. Mayr et al. cite Huber and Markgraf[16] stating "the pollen changes at Rio Rubens Bog are interpreted as eastward displacement of the forest-steppe limit as a response to decreasing fire frequency". In contrast to Mayr et al´s record, the Rio Rubens bog reveals pronounced long-term trends that imply a more westward located forest-steppe limit during the early Holocene, an expansion towards the east in the middle Holocene, and substantially more eastward location of this

DOI: 10.1038/NGEO959

Supplementary Information Lamy et al.
"Holocene changes in the position and intensity of the Southern Westerly wind belt"

limit in the late Holocene. These shifts could well be explained by enhanced early Holocene westerlies which caused especially an increase in evaporation and drought stress in austral summer with more fire-activity as observed by high charcoal contents[16]. This interpretation is consistent with additional pollen data from that site[17] showing traces (<2%) of *Drymis* and *Pseudopanax* that only appear during the early Holocene, when a stepparian vegetation (e.g Poaceae) dominated the landscape. These species are distinctive of humid and hyper-humid environments located to the west[18], and do not grow east of the Andes. The most plausible explanation would be that stronger westerly winds induced long-distance pollen transport to the site during the early Holocene consistent with our inferred wind enhancement.

Our major concern with the TDP records is the fact that these, primarily pollen-based studies assume a major control of rainfall on local vegetation[7-9]. Though the studies showed a positive rainfall-westerly wind strength relation also for this location already on the lee-side but relatively close to the Andean crest (based on the correlation NCEP-NCAR reanalysis precipitation to rainfall measured at a local weather station in TDP area), they largely miss the consideration of evaporation effects. We carefully studied the meteorological data from TDP (as shown in Moy et al.[8]). Though based only on a short time-series of 10 years, these data clearly show the dominating control of evaporation changes in particular during the vegetation period when evaporation/precipitation ratios reach values between 2 and 3 (see the figure below). Furthermore, the data reveal a clear positive and linear relation of evaporation to wind-strength in this area (see the figure below). We therefore suggest that vegetation changes in the TDP are strongly controlled by these evaporation changes in addition to possible effects of precipitation changes and the long-distance transport of pollen from further west where the positive rainfall-wind strength relation is even stronger than at TDP. Thus, we conclude that the interpretation of the TDP pollen records in terms of westerly wind strength is not straight-forward as stronger winds may increase precipitation but also evaporation which may result in paleo-vegetation changes that are difficult to explain.

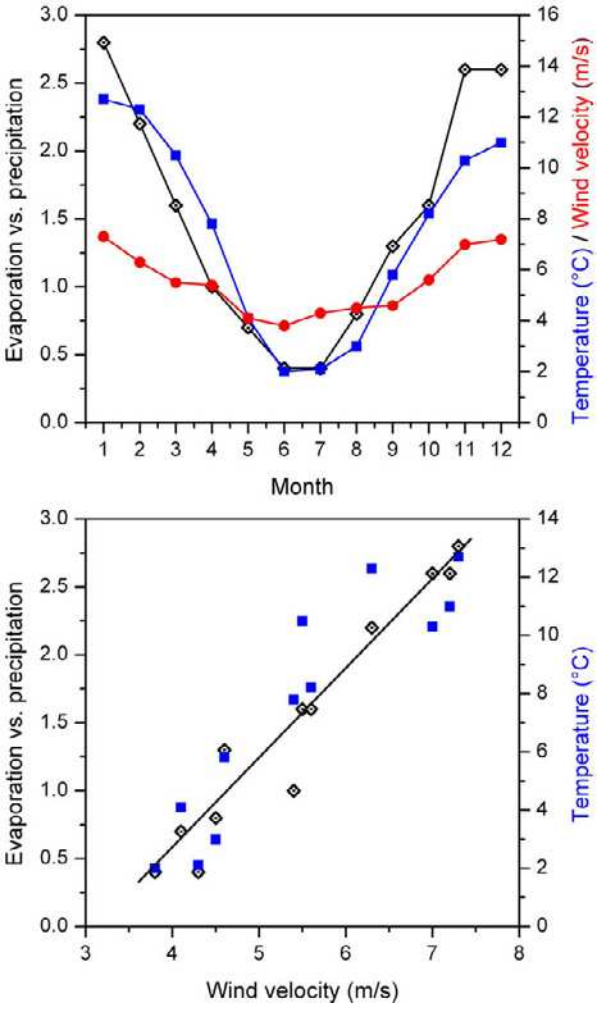

The upper panel shows evaporation/precipitation and temperature/wind velocity relations for TDP. Below, the apparently linear relationship between both temperature and evaporation/precipitation is shown. Data were graphically gripped from Fig. 2 in Moy et al.[8].

Taken together, at the climate transition zone to the east of the Andes (including likewise Lago Cardiel), there is no clear relationship between westerly wind intensity and available moisture for plants. Though there might be a weak positive relation between westerly wind strength and precipitation for e.g. TDP shown in the NCEP-NCAR data set (see e.g., Fig. 1 in Moy et al[8]), any potential impact on vegetation (used as proxy data) is strongly complicated by evaporation changes.

This is also important for the interpretation of lake levels in the rain shadow area of the Andes. In this region stronger westerly wind increases the effect of evaporation. In addition, during phases of less westerly wind influence, occasional easterly winds provide more Atlantic moisture to sites east of the Andes[4,15]). Therefore, not only vegetation changes, but also the interpretation of lake level variations (e.g. Lago Cardiel[3-5] and Laguna Potrok Aike[2]) are very difficult and often results in contradictory paleohydrological inferences.

Discussion on previously published Holocene westerly wind strength records from northern Patagonia and central Chile.

In contrast to the present core zone of the SWW in southern Patagonia, in northern Patagonia and central Chile numerous Holocene paleoenvironmental records are available from the windward (Chilean) side of the Andes. The paleoclimatic implications of these data have been recently summarised in a review article by Lattore et al.[19]. The available data clearly show dryer (and warmer) early Holocene and wetter (and mostly cooler) conditions during the late Holocene on the windward in the present winter-rain domain of central Chile extending southward to the island of Chiloe. On the eastern side of the Andes in Argentina (please refer to the review article by Mancini et al.[20]), several records show instead warm humid early Holocene conditions which would be consistent with a reduced lee-effect due to weaker westerlies at the northern margin. These weaker westerlies might have facilitated the inflow of Atlantic moisture to the Argentinean side of the Andes.

Supplementary Discussion 2

Methods, further details, and supporting data on the individual records

Core Sk1 (fjord)

Core Sk1 (52°37.31'S; 71°42.16'W, 62 m water depth) has been retrieved from the eastern part of Seno Skyring, a fjord system that extends from the Gran Campo Nevado mountain range (GCN) eastward into the eastern Andean foreland (Fig. 1). Present salinities are generally less than ~20 psu, i.e. too low for most carbonate producing marine organisms. Accordingly, the clayey-silty sediments in core Sk1 do not contain carbonate and are also barren of macroplant remains[21]. Therefore, the age model is based on 4 regional tephra layers (Supplementary Table S1) that have been radiocarbon dated in terrestrial environments in the area[22-24]. These tephra layers indicate relatively constant sedimentation rates for the whole sequence and provide reliable age control for our purpose of investigating multi-millennial trends over the Holocene. Due to the W-E elongation of the Skyring Fjord, westerly winds blowing over the Andean crest are channelized and enhanced. These winds induce a strong eastward surface flow capable of transporting clayey material from mafic metamorphic and plutonic Andean source rocks towards core location Sk1[21]. Clay mineralogical (illite- and chlorite-rich) and geochemical characteristics (relatively Mg- and K-rich) of these clays clearly support the long-distance advection from Andean sources in the GCN region >100 km to the west (Supplementary Fig. S2). Only very small input from local sources (smectite-dominated) in the semi-arid direct hinterland reaches the site during the early Holocene but higher smectite contents occur during the late Holocene when the wind-induced input of Andean clays is reduced (Supplementary Fig. S2)[21]. This pattern is consistent with clay mineralogical data of surface sediments and core-tops in the Skyring Fjord (Rolf Kilian unpublished data) clearly show the decreasing contents of illite and chlorite and increasing amounts of smectite within the Skyring fjord from west to east.

We use clay/silt ratios (clay 0.5-2µm; silt 2-63 µm; measured with a Galai CIS-1 laser particle counter) as a proxy for this wind-induced long-distance clay transport. We exclude a significant impact of Holocene glacier advances that may have supplied more glacial clay-bearing melt-water plumes at the head of the fjord system (GCN), because glaciers in this region were close to their modern extent by ~12.1 kyr BP (ref. 25) showing only minor advances in the late Holocene[26]. The relatively early glacial retreat is consistent with new data by Boyd et al.[27] clearly showing that the final deglaciation ended at ~12.5 kyr BP in the nearby Cordillera Darwin. Furthermore, data from Lake Chandler located only 6 km east of the present limit of the Gran Campo Nevado (GCN) ice-cap suggest that the glaciers were close to their modern limits at latest by ~12.1 kyr BP (ref. 25)

DOI: 10.1038/NGEO959

(Supplementary Fig. S6) but likely earlier as indicated by the onset of minerogenic peat formation at our site GC2 since at least 14 kyr BP (see GC2 below). Taken together, these different and independent evidences clearly suggest that glacier extent in the Strait of Magellan area was close to modern conditions at the beginning of the Holocene contradicting the view of McCulloch[28] who suggested that significant melting of the glacial ice-cap in the Strait of Magellan area extended into the early Holocene.

This interpretation is also supported by new data from Lago Argentino (Brazo Sur)[6] close to the eastern margin of the Southern Patagonian Ice Field clearly document that Early Holocene glacier advances were very restricted and much less pronounced than those of the late Holocene Neoglacial[29,30].

Therefore, we conclude that the Holocene clay/silt ratios of sediments from the Eastern Seno Skyring reflect the intensity of wind-induced eastward surface current transport of clays. Compared to the Late Holocene, two-fold higher clay/silt ratios in the Early Holocene indicate significantly enhanced westerly winds.

Core Palm2 (fjord)

Core Palm2 is situated west of the GCN at the northern margin of Bahia Beaufort (52°47.4'S, 73°38.9'W, 44 m water depth), ~70 km east of the western entrance of the Magellan Strait with a sill depth of ~40 m below present day sea-level. The age model is based on 2 radiocarbon ages and 4 well dated tephra layers (Supplementary Table S1). The area is characterised by a large W-E salinity decline in surface waters (0-~50 m water depth) from the open ocean towards the semi-enclosed inner fjord area (Glacier Bay) receiving considerable amounts of glacial meltwater[21].

We use the strongly varying (up to a factor of 4) $CaCO_3$ accumulation rates (AR) as a proxy for paleosalinity. $CaCO_3$ in the core is of biogenic origin (primarily benthic and to a lesser extent planktonic foraminifera) and reflects the influence of open marine Pacific waters. Present day observations show that periods of enhanced westerly winds (with higher precipitation) lower salinities at the Palm2 Site, as the low-salinity waters are kept within the fjord system and local rainfall supplies freshwater. In contrast, periods of reduced westerly winds and less rainfall weaken the low-salinity surface layer and enhance the influence of open marine waters at the core site. Studies on surface samples within this fjord system show the close relationship of biogenic $CaCO_3$ contents to salinity (Rolf Kilian, unpublished data). Major carbonate producers within the fjords are benthic foraminifera. Studies from surface sediments in the region showed that the abundance of calcareous benthic taxa clearly traces the open oceanic influence whereas agglutinated forms dominate in the inner fjords with lower salinities[31]. Eustatic sea-level was still rising in the early Holocene[32] and would have enhanced the inflow of open marine waters into the fjord system and thus would have resulted in higher salinities and biogenic carbonate production. Instead, we observe a decrease in biogenic $CaCO_3$ AR after the initial marine transgression phase between 14.3 to 13.5 kyr BP (ref. 25), lasting until the earliest Holocene and suggesting that fresh-water supply and wind forcing were the dominant processes in controlling paleosalinities at site Palm2 during the early and middle Holocene.

Core TM1 (fjord)

Coring site TM1 (52°53.37'S; 73°46.93'W, 31 m water depth) is located ~60 km east of the western entrance of the Magellan Strait in a small fjord bay close to Tamar Island. The age model is based on 4 radiocarbon and 2 well-dated tephra layers (Supplementary Table 1). In contrast to site Palm2, site TM1 is protected from the open fjords by shallow (~10-20 m water depth) sills. Therefore, paleosalinities are stronger affected by local isostatic rebound and sea-level changes making this proxy not suitable for wind/precipitation estimates at this location. Instead, site TM1 has a larger and more elevated catchment area including Magellanic Rainforest, peat-land, and non-vegetated rock surfaces (Supplementary Fig. S3). Therefore, we use the AR of terrigenous siliciclastic material and terrestrial organic carbon as paleo-precipitation proxies at this site.

Siliciclastic AR have been calculated from percentages of siliciclastic material (100 %-CaCO3 % - organic carbon % – biogenic opal %). Terrestrial organic carbon contents have been obtained from bulk organic carbon contents using

molar N/C ratios (both determined by standard methods). It has been recently shown that mixing equations based on C/N data underestimate the terrestrial fraction[33]. We therefore use N/C ratios which provide a linear relationship between terrestrial and marine derived organic carbon[33]. We use a molar N/C ratio of 0.17 (C/N=6) as the marine (micro-algal) end-member. This value is consistent with Holocene N/C ratios measured in open marine sediments from the continental slope off the Magellan Strait (core MD07-3128; Lamy et al., unpublished data) which do not receive any terrestrial input during the Holocene. Our terrestrial (vascular plant) end-member (molar N/C=0.033; C/N=30.6;) is based on the average values from 5 terrestrial mass flow layers in sediments from Tamar Lake (core TML1; see below) consisting of removed soils and vegetation fragments.

Due to the shallow sills around the fjord bay at site TM1, both siliciclastic and organic terrigenous material primarily originates from nearby sources on the surrounding land areas and is supplied during strong rainfall periods. Some long-distance transport of e.g. glacial clay from the GCN may have occurred before ~12 kyr BP (ref. 25) (Fig. 2d). During most of the Holocene, the comparatively high salinity of the western fjords caused clay flocculation, restricting the extension of glacial clay plumes to the inner fjords close to the GCN glaciers. Compared to late Holocene values, siliciclastic AR more than doubled and terrestrial organic carbon AR increased up to ten-fold during the early Holocene humid period.

Core TML1 (lake)

Core TML1 has been retrieved after systematic parametric sediment echosounding in the deepest part (22 m water depth) of the small Tamar Lake (0.72 km^2), located at an altitude of ~35 m above sea-level directly onshore site TM1 (52°54.21'S, 73°48.07`W). The lake catchment (2.3 km^2) includes peat bogs (Magellanic Moorland[18]) over the flat areas, and forests (Subantarctic Evergreen Forest[18]) over partly steeper slopes up to 430 m altitude (Supplementary Fig. S4).

The age model is based on 14 radiocarbon ages and 2 well-known tephra layers (Supplementary Table S1). The radiocarbon dates were all performed on plant material and provide a very reliable age-control for the lake record. The core contains 5 major terrestrial mass flow layers (13-34 cm thick) consisting of removed soils and vegetation fragments (Supplementary Fig. S3). These layers occur in the early Holocene section (between ~8.7 and 11.8 kyr BP, Fig. 2g) and are most likely related to extreme precipitation events during the early Holocene wet phase (as derived from higher terrestrial organic carbon contents and pollen indicators as discussed below). This inference is strongly supported by ecological studies developed in adjacent areas that indicate an erosional mechanism in peatlands living at high slopes, induced and controlled by runoff[34]. Our pollen data (see below) indicate ~2000 yrs of delay between the vegetation establishment, and the deposition of the first mass flow layer, further supporting a primary climate-driven mechanism in the mass flow layer genesis. In addition, there are numerous thinner (~0.3 to 5cm) layers primarily consisting of re-deposited glacial clay (Supplementary Fig. S3). We interpret these layers as storm event layers that originate from fine-sediment suspension in shallow near-shore parts of the lake where glacial clays are exposed. Both, the mass flows and storm event layers are clearly identifiable from visible core inspection. In addition, the storm event layers are seen as distinct lighter intervals in the sediment gray-scale record and minima in bulk organic carbon contents (Supplementary Fig. S3). Mass flows and storm event layers have been subtracted before calculating sedimentation-rates (Supplementary Table S1). As in core TM1, we use the AR of terrestrial organic carbon as our main paleo-precipitation proxy. Terrestrial organic carbon AR have been calculated as described for core TM1 using for TML1 an aquatic (limnic) end-member with a molar N/C value of 0.15 (C/N=6.7) (Supplementary Fig. S3). This value is based on N/C values from sediments at the base of the core deposited during the late glacial when soil and vegetation development has not yet started and terrestrial organic carbon input was negligible (Supplementary Fig. S3).

The lake and the fjord terrestrial organic carbon records reveal a similar long-term trend during the Holocene, though the early Holocene maximum in organic carbon AR extends into the middle Holocene in the lake record. Furthermore, a pronounced increase in organic carbon AR at ~4.2 kyr BP occurs only in the lake record. This

increase is related to the impact of the large Mt.-Burney eruption at this time that substantially enhanced terrestrial organic carbon supply due to tephra-related soil acidification[35].

In addition, our paleoclimatic inferences are strongly supported by pollen data. Sediment samples of 2 cc were processed for pollen analysis following standard techniques[36], and then mounted on pollen slides with glycerin. The pollen counting was realized at 400× and 1000× magnification utilizing a Leica DM-LB2 stereomicroscope. The basic pollen sum for each level includes at least 300 pollen grains of terrestrial origin. Percentages of aquatic and fern taxa were calculated from a super-sum that included the basic pollen sum, the aquatic taxa sum, and the Pteridophytes sum. Pollen and spore identifications were made utilizing reference material and literature[37,38].

The pollen record from TML (Supplementary Fig. S5) constitutes the first attempt to reconstruct the vegetational history from lake sediments on the windward side of the Andes in Southwest Patagonia. The preliminary data indicate important changes of the vegetational landscape during the past ~14,300 years in the study area. Plant colonization started immediately after the ice retreat suggesting a first minor warming pulse (coinciding with the lithological change from glacial clays to organic silt; Supplementary Fig. S3). High relative percentages of non-arboreal species (moorland vegetation) occur between ~14.3-13.2 kyr BP implying almost treeless vegetation, growing under relatively cold, moist and windy climatic conditions. The abrupt expansion of *Nothofagus dombeyi* type at ~13.2 kyr BP indicates the establishment of *Nothofagus* stands in the area under more temperate climatic conditions. Later, a distinct forest succession is observable, ranging from a *Nothofagus*-dominated forest (~13.2-9.3 kyr BP), to *Nothofagus-Drimys* forest (~9.3-5.2 kyr BP), and leading to the establishment of mixed evergreen forest (~5.2 kyr BP to present). The establishment of *Nothofagus-Drimys* forest and finally the mixed evergreen forest suggests an important precipitation decrease towards the late Holocene. This general paleoclimatic interpretation of the pollen data clearly supports a climatic interpretation of the high relative percentages of *Misodendron* during the more humid early Holocene (Fig. 2f). *Misodendron* is a hemiparasite that infests several *Nothofagus* species[39]. Higher abundance of *Misodendron* can be interpreted in terms of the presence of open *Nothofagus* forest growing under limited ecological conditions (e.g swamp soils). Moreover, the increase in the relative percentages of the aquatic fern *Isoetes* post ~8.5 kyr BP suggests a reduction of wind-stress over the lake surface. Today, *Isoetes* lives only in the shallow margins (<1 to 1.5 m) of lake Tamar. During high wind conditions the shores are seriously impacted affecting the *Isoetes* populations, and hence reducing the *Isoetes* pollen signal.

Core GC2 (peat bog)

The core has been recovered from a peat bog 8 km east of the present day GCN ice-cap in vicinity of Canal Gajardo on Peninsula Munoz Gamero at an altitude of ~70 m above sea-level (52°48.62´S; 72°55.77´W). The site is located in a small basin where peat bogs grew during the whole Holocene (except for a short hiatus after the 4.18-kyr Mt. Burney eruption[35]) (Supplementary Fig. S6).

The core reaches back to the late glacial and is dated by 9 radiocarbon dates (8 in the Holocene sequence) and includes the well-dated 4.18-kyr and 8.61 kyr Mt. Burney tephra layers (Supplementary Table S1). A further tephra layer originating from the Hudson volcano has been found in core GC2[22]. We use the well-dated framework of GC2 to constrain the age of the Hudson tephra layer that is likewise recognized in core Palm2 (Supplementary Table S1).

The pollen data have been previously published by Fesq-Martin et al.[40]. Detailed paleoclimatic interpretations are, however, not given by these authors. We therefore provide a new summary pollen diagram based on the published data (Supplementary Fig. S6) including the three major pollen groups that represent characteristic vegetational formations living in the study area: Trees (primarily *Nothofagus* and *Drymis winteri*), shrubs and herbs (i.e., *Gunnera*, Ranunculaceae, *Pernettya* and Asteraceae), and hygrophytes (i.e., Cyperaceae, Juncaceae, *Astelia*, *Donatia* and Pteridophyta). Furthermore, we include the total pollen concentration. Plant colonization starts immediately after the ice retreat (~14.4 kyr BP), coeval with our pollen record from Lake Tamar

Supplementary Information Lamy et al.
"Holocene changes in the position and intensity of the Southern Westerly wind belt"

(TML1), suggesting an initial warm pulse. The initial pollen assemblage (~14.4-11 kyr BP) is dominated by shrubs and herbs, mainly *Gunnera magellanica* a typical pioneer species that lives in recently ice-free areas. Low total pollen concentrations during this period indicate a treeless landscape.

Within the super-humid environment of the GCN area with annual rainfall of 5000 to >10000 mm/a[11], we interpret in particular the amount of the hygrophytic plant species as a sensitive proxy for Holocene precipitation changes. The area is characterised by a roche moutonnée landscape with a number of small depressions (Supplementary Fig. S7). During periods of long-lasting and strong rainfall, stagnant moisture produces small lakes. These lakes can then occupied by hygrophytes which we use as a proxy for more humid intervals. The percentage of hygrophytes abruptly increases at ~11 kyr BP. As shown by our other records (including the pollen record from TML1), rainfall already started to increase before, at ~ 12.5 kyr BP (Fig. 2). We suggest a delayed response of the GC2 pollen record due to slowly evolving soils and peat bogs near a local glacier of the GCN ice-field that remained close to the pollen site until ~11 kyr BP. Though with relatively large fluctuations, hygrophyte concentrations remain high until ~8.5 kyr BP when tree pollen start to increase. This forest expansion illustrates a decrease in the precipitation, restricting the environment where the hygrophytes live.

DOI: 10.1038/NGEO959

Supplementary Information Lamy et al.
"Holocene changes in the position and intensity of the Southern Westerly wind belt"

Supplementary Fig. S1

Modern climate in the study area. Left panel shows map of local correlation between monthly anomalies of precipitation and 850-hPa zonal wind (after ref. 41) (green star shows location of study area). Right panel shows seasonal pattern of monthly average precipitation and monthly average wind velocities at the Gran Campo Nevado weather station in the centre of our study area(ref. 11 and Rolf Kilian; unpublished data).

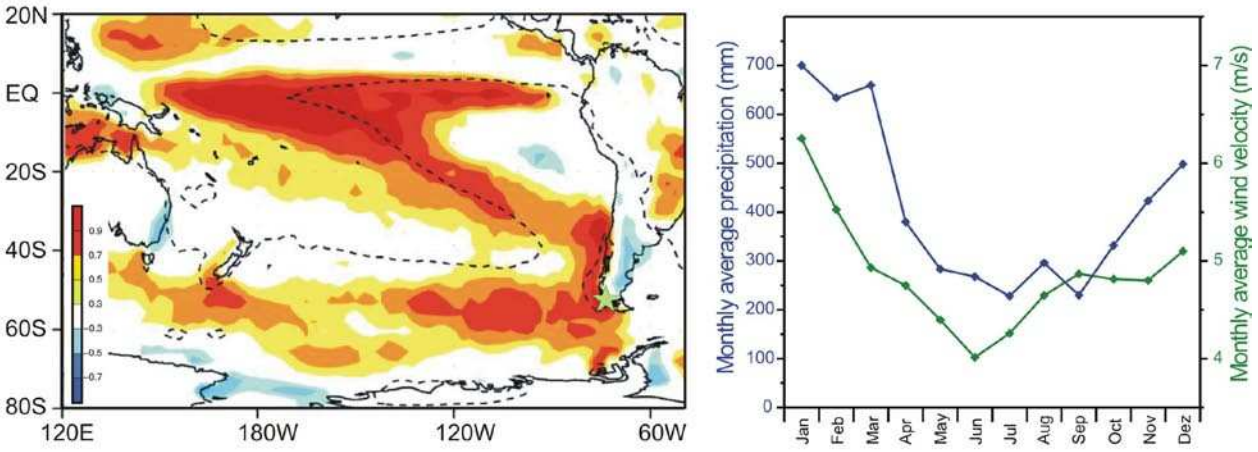

Supplementary Information Lamy et al.
"Holocene changes in the position and intensity of the Southern Westerly wind belt"

Supplementary Fig. S2

Supporting geochemical and clay mineralogical data of core SK1. **a**, clay/silt ratio as shown in Fig. 2b. b, MgO content of the bulk sediment. **c**, K_2O content of the bulk sediment. **d**, chlorite content. **e**, illite content. **f**, smectite content. Vertical bars mark the multi-millennial Holocene periods as shown in the main text. Here, we extend the figure back to 15 kyr BP showing the deglacial interval (gray bar) with substantial input of glacial clay that ceases between ~12.5 and ~12.1 kyr BP.

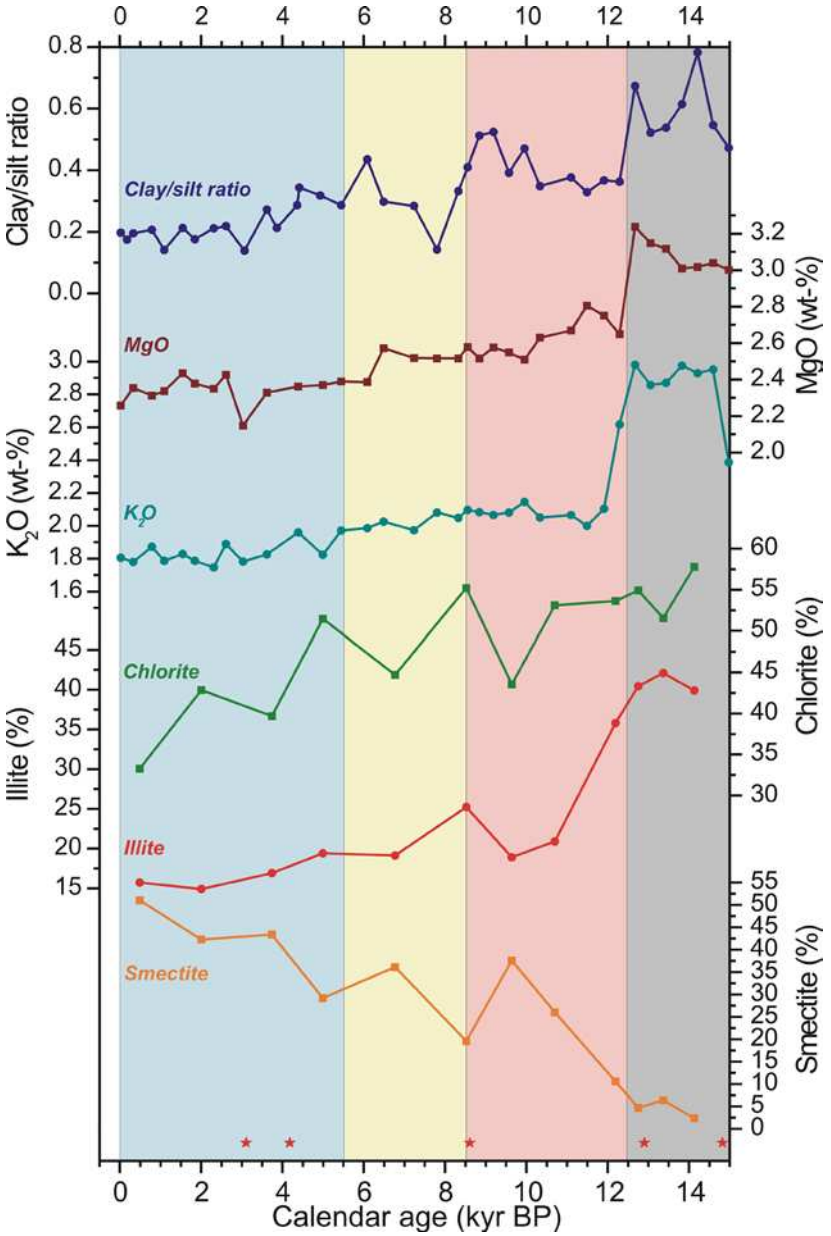

DOI: 10.1038/NGEO959

Supplementary Information Lamy et al.
"Holocene changes in the position and intensity of the Southern Westerly wind belt"

Supplementary Fig. S3

Gray-scale, bulk organic carbon and molar C/N ratio records from core TML1 versus uncorrected core depth. Gray curve shows gray-scale record with distinct lighter layers representing storm deposits (marked as light brown bars below). Yellow-brown bars mark terrestrial mud flow layers and dark-brown bars the two tephras originating from eruptions of Mt.-Burney. Blue open diamonds show bulk organic carbon contents with minima in storm event layers. Blue line connects data points from the undisturbed intervals used for calculating terrestrial organic carbon AR (Fig. 2f). Red diamonds show molar C/N ratios with red line connecting the data points from background sedimentation intervals. Yellow bar at the top marks C/N values from terrestrial mud flow layers used for defining the terrestrial end-member. Green bar marks two data points from the base of the core (late glacial) taken as the aquatic (limnic) end-member.

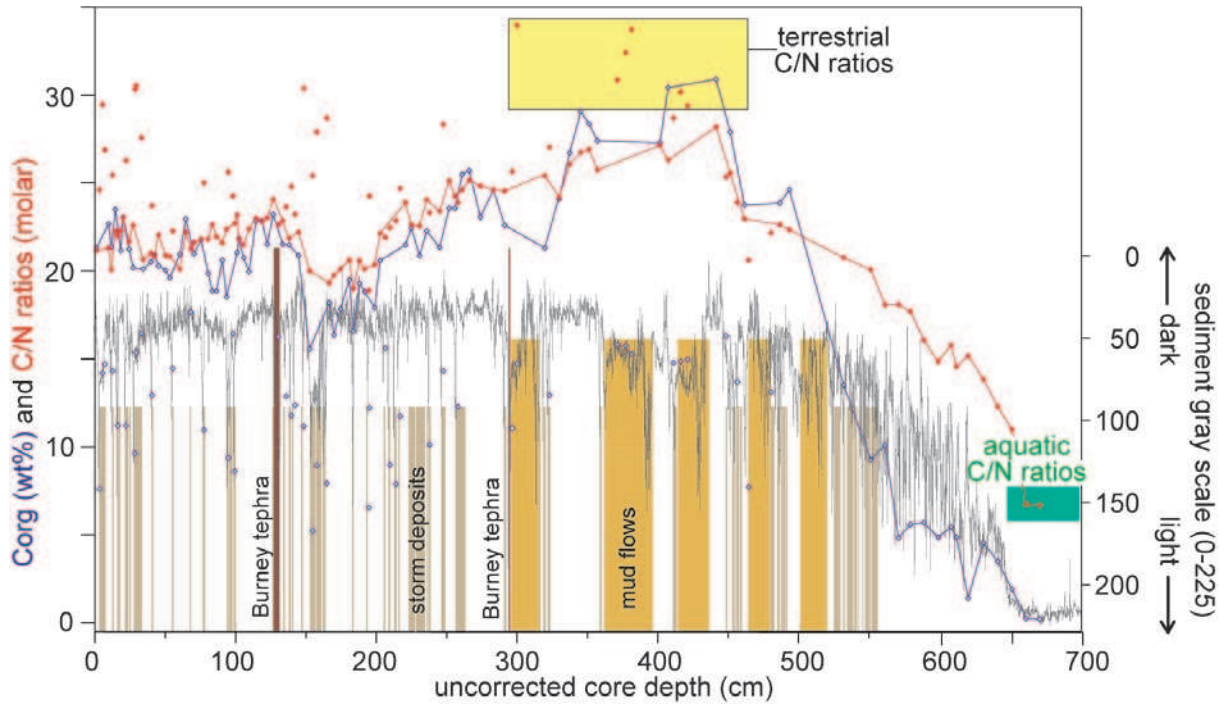

Supplementary Information Lamy et al.
"Holocene changes in the position and intensity of the Southern Westerly wind belt"

Supplementary Fig. S4

Physiographic setting of site TML1 (Tamar lake) and TM1 (fjord). **a** , Panoramic view of the area (photo Helge Arz). **b**, Schematic image of the main plant formations.

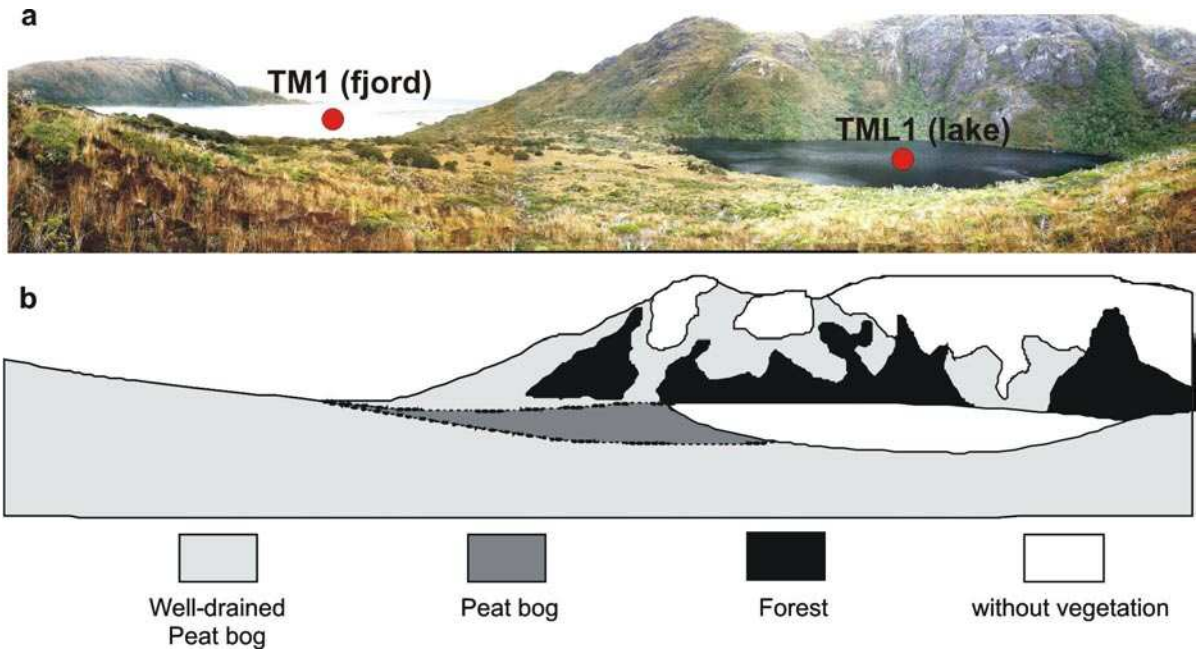

DOI: 10.1038/NGEO959

Supplementary Information Lamy et al.
"Holocene changes in the position and intensity of the Southern Westerly wind belt"

Supplementary Fig. S5

Additional pollen data from core TML1. The expansion of *Nothofagus*, *Drimys* and other tress indicates the forest succession ranging from a *Nothofagus* forest (~13.2-9.3 kyr BP), to *Nothofagus-Drimys* forest (~9.3-5.2 kyr BP), and leading to the establishment of mixed evergreen forest (~5.2 kyr BP to present). We utilize *Misodendron* as an indication of *Nothofagus* growing under stress condition by waterlogging. Increases in the relative percentages of the aquatic fern *Isoetes* post ~8.5 kyr BP suggest a reduction of the wind-stress over the lake surface (further information in Supplementary Discussion 2).

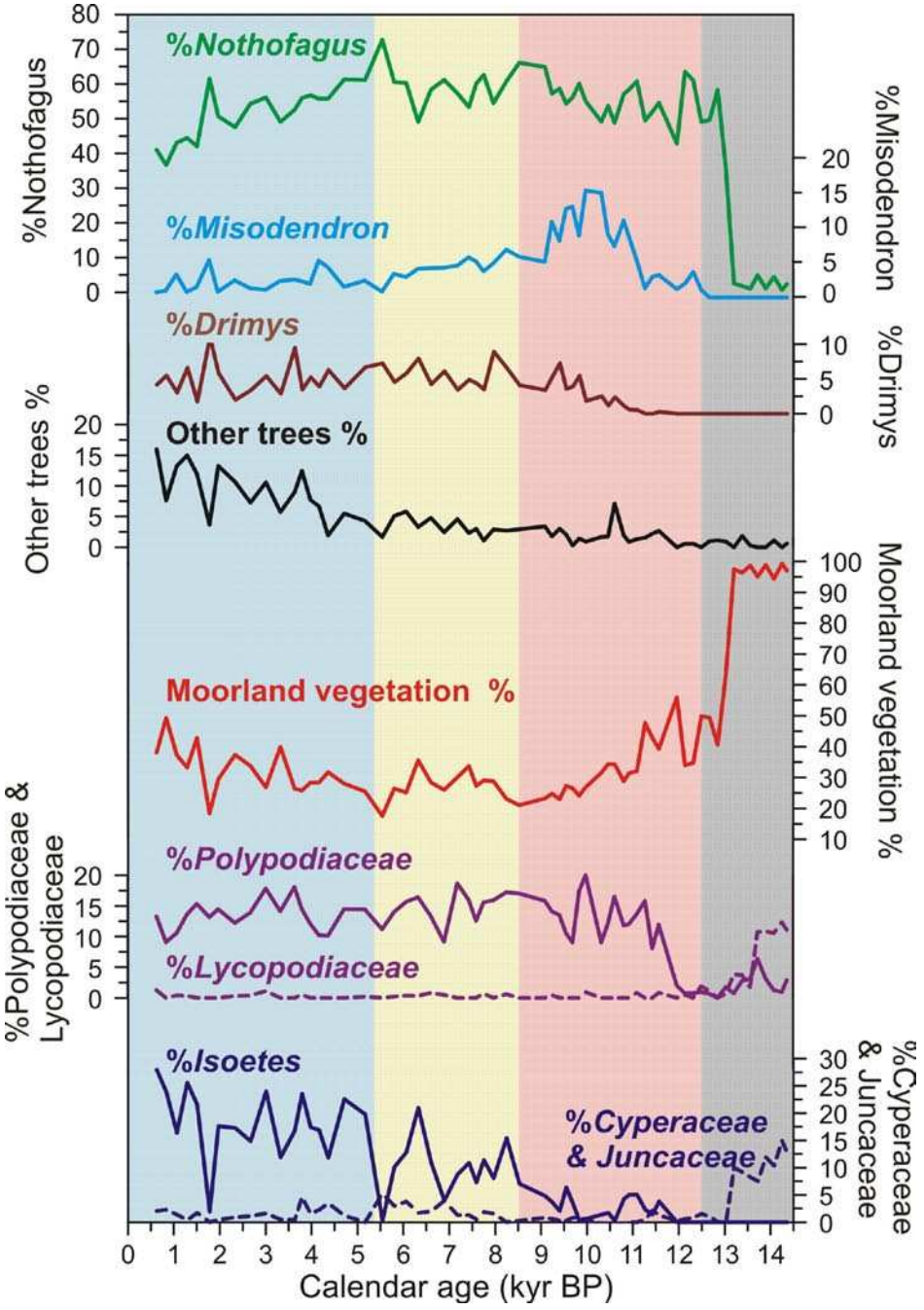

Supplementary Information Lamy et al.
"Holocene changes in the position and intensity of the Southern Westerly wind belt"

Supplementary Fig. S6

Additional pollen data from peat-bog core GC2. Based on the pollen countings of Fesq-Martin et al.[40], relative pollen percentages of the major vegetation groups trees, shrubs/herbs, and hygrophytes together with the total pollen concentration are shown (further information in Supplementary Discussion 2 and on Supplementary Fig. S7).

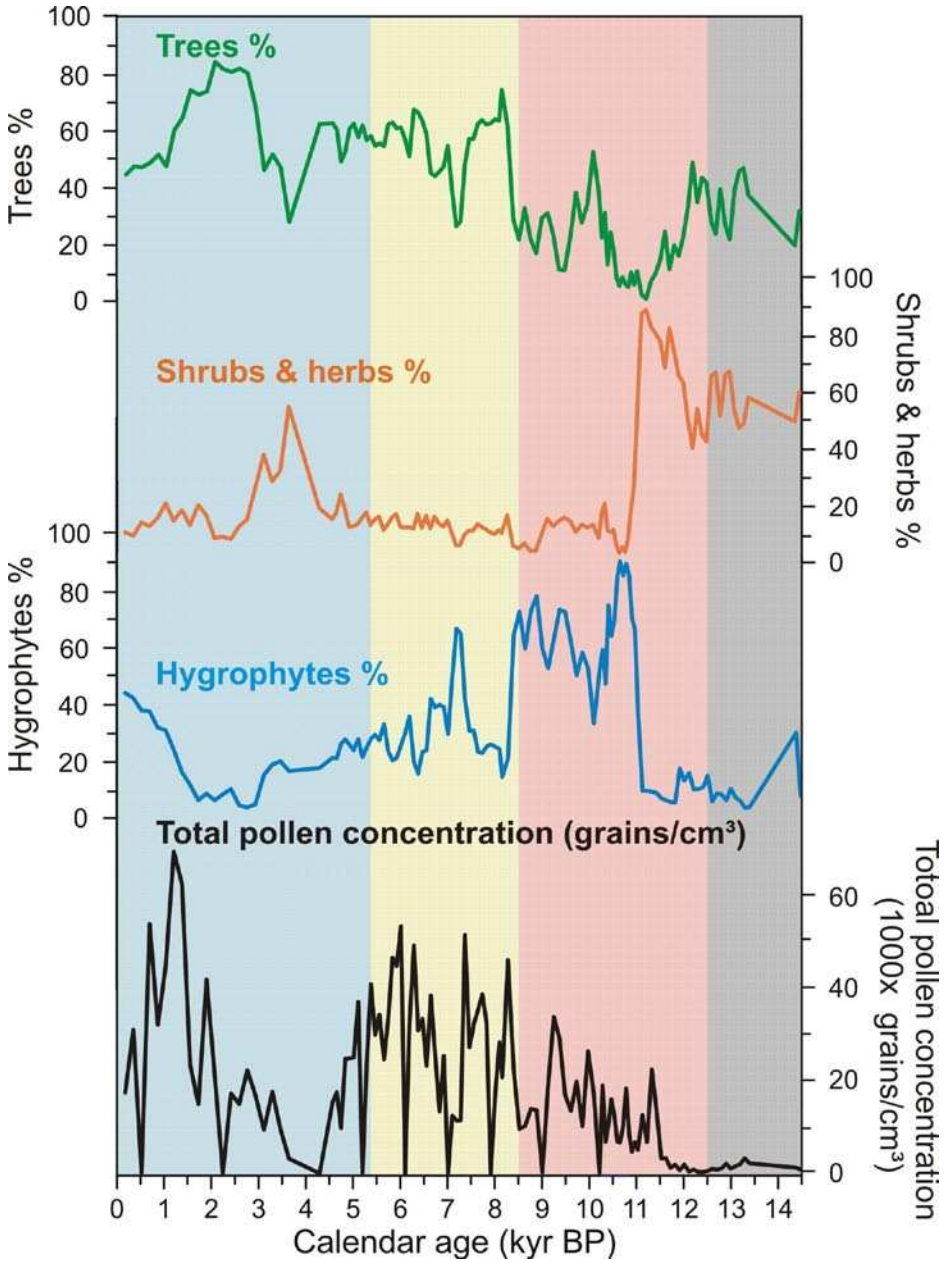

DOI: 10.1038/NGEO959

Supplementary Information Lamy et al.
"Holocene changes in the position and intensity of the Southern Westerly wind belt"

Supplementary Fig. S7

Physiographic setting of site GC1 (peat bog) showing location of site in a roche moutonnée landscape with a number of small depressions (Photo: Rolf Kilian). During periods of long-lasting and strong rainfall, stagnant moisture produces small lakes. These lakes can then occupied by hygrophytes which we use as a proxy for more humid intervals.

Also shown is the glacier extent in the area at ~12.1 kyr BP only ~5 km east of the modern glacier tongue. This data is consistent with the transition of glacial clay to organic sedimentation recorded at Lake Chandler (CH1)[25]. Taken together, these data suggest that glaciers where very close to modern conditions at the beginning of the Holocene. However, the decaying ice-sheet has influenced the plant evolution around site GC2 until ~11 kyr BP (see Supplementary Discussion 2).

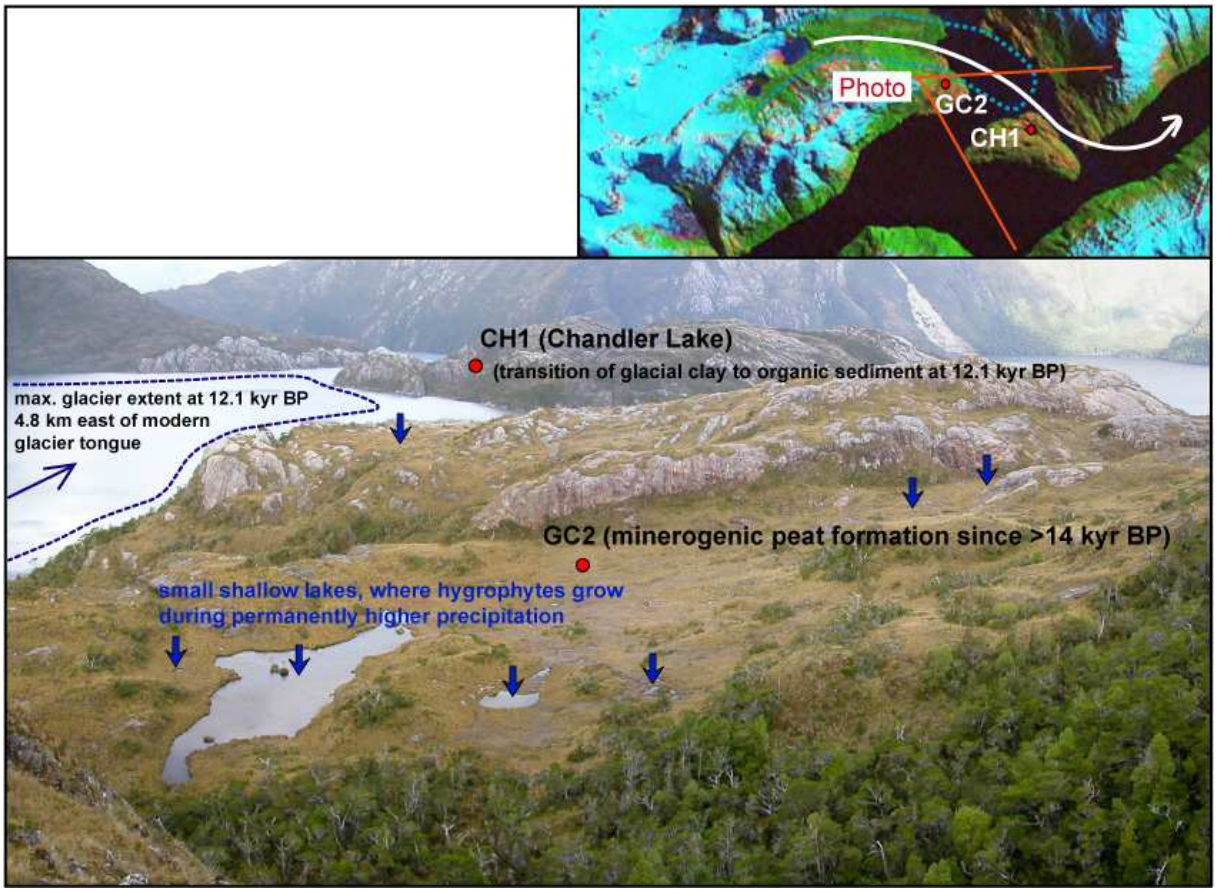

Supplementary Information Lamy et al.
"Holocene changes in the position and intensity of the Southern Westerly wind belt"

Supplementary Fig. S8

Supporting modern climatological data. Annual cycles of 850 hPa zonal wind (top), SST anomaly from annual mean (middle), and meridional SST gradient (bottom) zonally averaged over the Pacific region (150°E-70°W) in the southern hemisphere. Long-term monthly-mean climatologies based on NCEP/NCAR (wind)[42] and NODC World Ocean Atlas 1998 (SST). Spatial resolutions are 2.5° (wind) and 1° (SST, SST gradient).

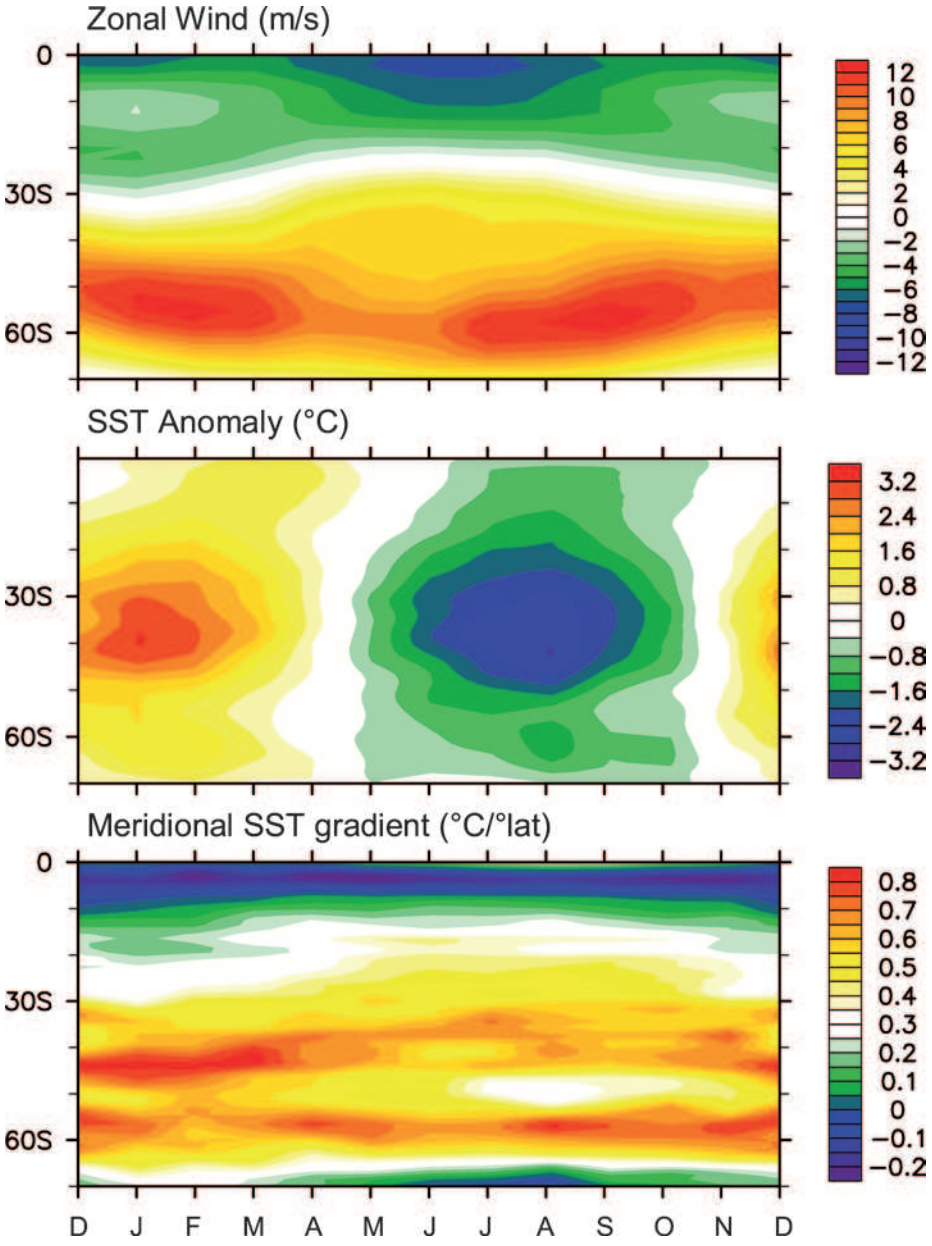

DOI: 10.1038/NGEO959

Supplementary Information Lamy et al.
"Holocene changes in the position and intensity of the Southern Westerly wind belt"

Supplementary Table S1

Age control points

Core depth[#]	Material	^{14}C age (yr BP)	Error (± yr)	Calibrated age (yr BP)*	Sed.-rate (cm/kyr)	References
Sk1						
0				-50		Modern age
83	Aguilera tephra	3000	100	3105	26	ref. 24
100	Mt. Burney tephra	3860	50	4185	16	ref. 23
177	Mt. Burney tephra	7890	45	8610	17	ref. 22
339	Reclus tephra	12685	260	14820	26	ref. 24
Palm 2						
0				-50		Modern age
185	marine shell	2570	30	2410	75	this paper
292	Mt. Burney tephra	3860	50	4185	60	ref. 23
351	Mt. Burney tephra			5690	39	Interpolated age (ref. 22)
463	Hudson tephra			8090	47	Interpolated age (ref. 22)
482	Mt. Burney tephra	7890	45	8610	37	ref. 23
590	marine shell	10240	60	11690	35	this paper
TM1						
0				-50		Modern age
96	Mt. Burney tephra	3860	50	4185	23	ref. 23
112	marine shell	4550	40	4970	20	ref. 21
142	marine shell	5550	35	6090	27	this paper
220	Mt. Burney tephra	7890	45	8610	31	ref. 22
238	marine shell	8430	50	9200	31	ref. 21
434	marine shell	11720	60	13310	48	ref. 21
TML1						
0				-50		Modern age
26.7	Plant remain	1075	30	940	27	This paper
36.9	Plant remain	1380	40	1250	33	This paper
46.9	Plant remain	1745	40	1595	29	This paper
63.3	Plant remain	2295	30	2240	26	This paper
88.2	Plant remain	3000	30	3130	28	This paper
104.9	Plant remain	3525	40	3760	27	This paper
122.9	Mt. Burney tephra	3860	50	4185	42	ref. 23
131.8	Plant remain	4040	130	4445	34	This paper
182.6	Plant remain	5715	35	6445	25	This paper
211.4	Plant remain	6520	65	7370	31	This paper
230.2	Plant remain	7100	200	7850	39	This paper
252.2	Plant remain	7750	50	8480	35	This paper
256	Mt. Burney tephra	7890	45	8610	29	ref. 22

Supplementary Information Lamy et al.
"Holocene changes in the position and intensity of the Southern Westerly wind belt"

Core depth#	Material	^{14}C age (yr BP)	Error (± yr)	Calibrated age (yr BP)*	Sed.-rate (cm/kyr)	References
TML1						
281.5	Plant remain	8410	55	9380	33	This paper
333.7	Plant remain	9640	70	10935	34	This paper
393.4	Plant remain	11020	40	12870	31	This paper
GC2						
0				-50		Modern age
31	Plant remain	2620	30	2690	11	ref. 40
41	Plant remain	3280	45	3430	14	ref. 40
42	Mt. Burney tephra	3860	50	4185	1	ref. 23
116	Plant remain	6915	40	7690	21	ref. 22
133	Plant remain	7290	70	8060	46	ref. 40
134	Hudson tephra			8090	33	Interpolated age, this study
144	Plant remain	7635	40	8390	33	ref. 22
150	Mt. Burney tephra	7890	45	8610	27	ref. 22
165	Plant remain	9020	80	10080	10	ref. 40
191	Plant remain	9660	85	10950	30	ref. 40
195	Plant remain	9740	40	11110	25	ref. 40
269	Plant remain	12020	200	13890	27	ref. 40

#Core depths are corrected for tephra layers > 1cm thickness and missing modern sediment surfaces through appendix of gravity cores. For core TML1, core depths were corrected for terrestrial mass flow and storm event layers (Supplementary Fig. S3).

*Radiocarbon samples have been calibrated using Calib5.1 and the SHCal04 Southern Hemisphere calibration data-set[43]. For ages beyond the SHCal04 calibration curve, we used the IntCal04 calibration curve and subtracted 60 years from the IntCal04 calendar age[43]. For the marine shells in core Palm2 and TM1, a reservoir correction of 200 years has been applied that provided the best agreement with the independently dated tephra layers in the cores[25]. The ages of tephra layers are based on radiocarbon dates in terrestrial environments (lakes and peat bogs) and are thus independent of marine reservoir age assumptions[22-24].

DOI: 10.1038/NGEO959

Supplementary Information Lamy et al.
"Holocene changes in the position and intensity of the Southern Westerly wind belt"

References for Supplementary Information

1 Mayr, C. *et al.* Holocene variability of the Southern Hemisphere westerlies in Argentinean Patagonia (52 degrees S). *Quaternary Science Reviews* **26**, 579-584 (2007).

2 Haberzettl, T. *et al.* Lateglacial and Holocene wet-dry cycles in southern Patagonia: chronology, sedimentology and geochemistry of a lacustrine record from Laguna Potrok Aike, Argentina. *Holocene* **17**, 297-310 (2007).

3 Gilli, A. *et al.* Mid-Holocene strengthening of the Southern westerlies in South America - Sedimentological evidences from Lago Cardiel, Argentina (49 degrees S). *Global and Planetary Change* **49**, 75-93, doi:DOI 10.1016/j.gloplacha.2005.05.004 (2005).

4 Markgraf, V. *et al.* Holocene palaeoclimates of southern Patagonia: Limnological and environmental history of Lago Cardiel, Argentina. *Holocene* **13**, 581-591 (2003).

5 Wenzens, G. Glacier advances east of the Southern Andes between the Last Glacial Maximum and 5,000 BP compared with lake terraces of the endorrheic Lago Cardiel (49 S, Patagonia, Argentina). *Z. Geomorph.* **N.F. 49**, 433454 (2005).

6 Wille, M. & Schäbitz, F. Late-glacial and Holocene climate dynamics at the steppe/forest ecotone in southernmost Patagonia, Argentina: The pollen record from a fen near Brazo Sur, Lago Argentino. *Vegetation History and Archaeobotany* **18**, 225-234 (2009).

7 Moreno, P. I., Francois, J. P., Villa-Martinez, R. P. & Moy, C. M. Millennial-scale variability in Southern Hemisphere westerly wind activity over the last 5000 years in SW Patagonia. *Quaternary Science Reviews* **28**, 25-38 (2009).

8 Moy, C. M. *et al.* Isotopic evidence for hydrologic change related to the westerlies in SW Patagonia, Chile, during the last millennium. *Quaternary Science Reviews* **27**, 1335-1349 (2008).

9 Moreno, P. I., Francois, J. P., Moy, C. M. & Villa-Martinez, R. Covariability of the Southern Westerlies and atmospheric CO2 during the Holocene. *Geology* **38**, 727-730, (2010).

10 Carrasco, J. F., Casassa, G. & Rivera, A. in *The Patagonia Icefield.* eds G. Cassassa, F. Sepulveda, & R. Sinclair) 29-41 (Kluwer-Plenum, 2002).

11 Schneider, C. *et al.* Weather observations across the Southern Andes at 53(degrees)S. *Phys. Geogr.* **24**, 97-119 (2003).

12 Rosenblüth, B., Casassa, G. & Fuenzalida, H. Recent climate changes in western Patagonia. *Bulletin of Glacier Research* **13**, 127-132 (1995).

13 Rasmussen, L. A., Conway, H. & Raymond, C. F. Influence of upper air conditions on the Patagonia icefields. *Global and Planetary Change* **59**, 203-216 (2007).

14 Endlicher, W. Patagonien - klima- und agrarökologische Probleme an der Magellanstraße. *Geographische Rundschau* **43**, 143-151 (1991).

15 Wagner, S. *et al.* Transient simulations, empirical reconstructions and forcing mechanisms for the Mid-holocene hydrological climate in southern Patagonia. *Clim. Dyn.* **29**, 333-355 (2007).

16 Huber, M. & Markgraf, V. in *Fire and Climatic Change in Temperate Ecosystems of the Western Americas.* eds T.T. Veblen, W.L. Baker, G. Montenegro, & T.W. Swetnam) 357–380 (Springer, 2003).

17 Huber, U. M. *Linkage among climate, vegetation andfire in Fuego-Patagonia during the Late-glacial and Holocene*, University of Colorado at Boulder, (2001).

18 Pisano, E. Fitogeografía de Fuego-Patagonia Chilena. 1: Comunidades vegetales entre las latitudes 52º y 56ºS. *Anales del Instituto de la Patagonia* **8**, 121-150 (1977).

19 Latorre, C. *et al.* in *The Geology of Chile* eds T. Moreno & W. Gibbons) 309-328 (The Geological Society, 2007).

20 Mancini, M. V., Prieto, A. R., Paez, M. M. & Schäbitz, F. in *Developments in Quaternary Science* Vol. Volume 11 (ed J. Rabassa) 351-367 (Elsevier, 2008).

21 Kilian, R. *et al.* Late Pleistocene to Holocene marine transgression and thermohaline control on sediment transport in the western Magellanes fjord system of Chile (53 degrees S). *Quaternary International* **161**, 90-107 (2007).

Supplementary Information Lamy et al.
"Holocene changes in the position and intensity of the Southern Westerly wind belt"

22 Kilian, R., Hohner, M., Biester, H., Wallrabe-Adams, H. J. & Stern, C. R. Holocene peat and lake sediment tephra record from the southernmost Chilean Andes (53-55 degrees S). *Revista Geologica De Chile* **30**, 23-37 (2003).

23 McCulloch, R. D. & Davies, S. J. Late-glacial and Holocene palaeoenvironmental change in the central Strait of Magellan, southern Patagonia. *Palaeogeography Palaeoclimatology Palaeoecology* **173**, 143-+ (2001).

24 Stern, C. R. Holocene tephrochronology record of large explosive eruptions in the southernmost Patagonian Andes. *Bulletin of Volcanology* **70**, 435-454 (2008).

25 Kilian, R. *et al.* Palaeoecological constraints on late Glacial and Holocene ice retreat in the Southern Andes (53 degrees S). *Global and Planetary Change* **59**, 49-66 (2007).

26 Koch, J. & Kilian, R. 'Little Ice Age' glacier fluctuations, Gran Campo Nevado, southernmost Chile. *Holocene* **15**, 20-28 (2005).

27 Boyd, B. L., Anderson, J. B., Wellner, J. S. & Fernandez, R. A. The sedimentary record of glacial retreat, Marinelli Fjord, Patagonia: Regional correlations and climate ties. *Marine Geology* **255**, 165-178 (2008).

28 McCulloch, R. D. *et al.* Climatic inferences from glacial and palaeoecological evidence at the last glacial termination, southern South America. *Journal of Quaternary Science* **15**, 409-417 (2000).

29 Glasser, N. F., Harrison, S., Winchester, V. & Aniya, M. Late Pleistocene and Holocene palaeoclimate and glacier fluctuations in Patagonia. *Global and Planetary Change* **43**, 79-101 (2004).

30 Mercer, J. H. Glacial history of southernmost South America. *Quaternary Research* **6**, 125-166 (1976).

31 Hromic, T., Ishman, S. & Silva, N. Benthic foraminiferal distributions in Chilean fjords: 47 degrees S to 54 degrees S. *Marine Micropaleontology* **59**, 115-134 (2006).

32 Fleming, K. *et al.* Refining the eustatic sea-level curve since the Last Glacial Maximum using far- and intermediate-field sites. *Earth and Planetary Science Letters* **163**, 327-342 (1998).

33 Perdue, E. M. & Koprivnjak, J. F. Using the C/N ratio to estimate terrigenous inputs of organic matter to aquatic environments. *Estuar. Coast. Shelf Sci.* **73**, 65-72 (2007).

34 Roig, F. A., Dollenz, O. & Méndez, E. in *Transecta botánica de la Patagonia Austral.* eds O. Boelcke, D. Moore, & F. A. Roig) 457-519 (Consejo Nacional de Investigaciones Científicas y Técnicas, 1985).

35 Kilian, R. *et al.* Millennium-scale volcanic impact on a superhumid and pristine ecosystem. *Geology* **34**, 609-612 (2006).

36 Fægri, K. & Iversen, J. *Textbook of pollen analysis. London, United Kindgdom, John Wiley & Sons Ld. 327*. (John Wiley & Sons, 1989).

37 Heusser, C. J. *Pollen and spores of Chile, Modern types of the Pteridophyta, Gymnospermae, and Angiospermae. USA. 176 pages*. (The University of Arizona Press, 1971).

38 Markgraf, V. & D'Antoni, H. *Pollen Flora of Argentina*. (University of Arizona Press, 1978).

39 Markgraf, V., D'Antoni, H. & Ager, T. Modern pollen dispersal in Argentina. *Palynology* **5**, 235-254 (1981).

40 Fesq-Martin, M., Friedmann, A., Peters, M., Behrmann, J. & Kilian, R. Late-glacial and Holocene vegetation history of the Magellanic rain forest in southwestern Patagonia, Chile. *Vegetation History and Archaeobotany* **13**, 249-255 (2004).

41 Garreaud, R. D. Precipitation and circulation covariability in the extratropics. *Journal of Climate* **20**, 4789-4797 (2007).

42 Kalnay, E. *et al.* The NCEP/NCAR 40-year reanalysis project. *Bulletin of the American Meteorological Society* **77**, 437-471 (1996).

43 McCormac, F. G. *et al.* SHCal04 Southern Hemisphere calibration, 0-11.0 cal kyr BP. *Radiocarbon* **46**, 1087-1092 (2004).